JPE 19-1-16

https://doi.org/10.6113/JPE.2019.19.1.168
ISSN(Print): 1598-2092 / ISSN(Online): 2093-4718

Double-Objective Finite Control Set Model-Free Predictive Control with DSVM for PMSM Drives

Beishi Zhao*, Hongmei Li†, and Jingkui Mao*

†,*Department of Electrical Engineering and Automation, Hefei University of Technology, Hefei, China

Abstract

Discrete space vector modulation (DSVM) is an effective method to improve the steady-state performance of the finite control set predictive control for permanent magnet synchronous motor drive systems. However, it requires complex computations due to the presence of numerous virtual voltage vectors. This paper proposes an improved finite control set model-free predictive control using DSVM to reduce the computational burden. First, model-free deadbeat current control is used to generate the reference voltage vector. Then, based on the principle that the voltage vector closest to the reference voltage vector minimizes the cost function, the optimal voltage vector is obtained in an effective way which avoids evaluation of the cost function. Additionally, in order to implement double-objective control, a two-level decisional cost function is designed to sequentially reduce the stator currents tracking error and the inverter switching frequency. The effectiveness of the proposed control is validated based on experimental tests.

Key words: Double-objective control, Finite control set predictive control, Low computation complexity, PMSM drive system

I. INTRODUCTION

Permanent magnet synchronous motors (PMSMs) are widely used in electric vehicles (EVs). The current control performance is important to achieve high-performance control of PMSM drive systems. Model predictive control (MPC) presents clear physical concepts, a high dynamic response and a flexible control structure. With the rapid development of microcontrollers [1], this control has become increasingly popular and has been applied in PMSM drive systems. MPC can be classified into two types, continuous control set model predictive control (CCS-MPC) and finite control set model predictive control (FCS-MPC) [2]. CCS-MPC transforms the control problem into a quadratic programming problem. However, its complex computations brings difficulties in practical implementation. Thus, it is usually combined with an explicit solution that computes most of the optimization problem offline [3]. Unlike CCS-MPC, FCS-MPC considers the discrete nature of power converters and microprocessors, which includes restrictions and nonlinearities in a very intuitive way. The optimization problem is solved by using all of the candidate control states to predict the system state and by evaluating the results with a predefined cost function. Therefore, it is easier to realize real-time control. However, there are various uncertainties and disturbances in PMSM drive systems, which lead to a mismatch of the prediction model. In addition, if only the basic voltage vector is applied for a control period, an undesired current ripple appears.

Model-free control (MFC) [4] establishes the ultra-local model online based on the input and output of a system, and it uses this model to design the controller. This method has the advantages of strong robustness and high control performance due to its independence from a mathematical model of the controlled system, and it is applied in the deadbeat predictive current control of a PMSM drive system to tackle both inverter nonlinearity and parametric uncertainties [5].

During the past several years, many control techniques have been proposed to enhance the steady-state performance of FCS-MPC based control systems. Duty cycle control, which applies an active and a zero voltage vector during one control period, is one of these methods. The general method uses every active voltage vector to evaluate the cost function, and then calculates the duty cycle of the optimal active voltage vector [6], [7]. Therefore, it requires a lot of iterations.

Manuscript received May 9, 2018; accepted Nov. 6, 2018
Recommended for publication by Associate Editor Zheng Wang.
†Corresponding Author: hongmei.li@hfut.edu.cn
Tel: +86-551-62901418, Hefei University of Technology
*Dept. of Electrical Eng. and Automation, Hefei Univ. of Tech., China

The scheme is improved in [8]. The duty cycles of three directions are calculated efficiently, and the optimal one is determined by comparing the values of three duty cycles. To minimize global torque ripple, the optimization problem is solved through predicting the root-mean-square (RMS) value of the torque ripple over the entire control period [9].

However, the combination of a single active vector and a zero vector has a limited effect on improving steady-state control performance. Theoretically, in order to realize error-free tracking control, two adjacent active vectors and zero vectors need to be applied in a control period [10]. Therefore, three-vector-based FCS-MPC is used to improve the steady-state performance of power converters [11] and PMSM systems [12], [13]. Although these methods perform well, their computation process is complex. Moreover, they ensure steady-state performance at the cost of a high inverter switching frequency, which leads to a decline in system efficiency.

Discrete space vector modulation (DSVM) was introduced in [14] to improve the control performance of induction motors. The application of DSVM has been extended to FCS-MPC [15] and deadbeat control [16] to reduce the torque ripple of PMSMs. In [15], a new control set with real voltage vectors and virtual voltage vectors is used to evaluate the cost function. With the aim of reducing the computational burden, deadbeat torque control [16] is utilized to calculate the reference voltage vector (RVV). The optimal solution only enumerates three voltage vectors close to the RVV. However, the selection of weighting factors in the cost function is based on a large number of experiments, and the switching frequency of the inverter and the steady-state control performance cannot be optimized simultaneously.

One of the advantages of FCS-MPC is that it is easy to handle multi-objective control problems. The switching losses of power devices reduce system efficiency. Therefore, a control method with a low switching frequency is valuable [17]. Multi-objective control considering a switching frequency reduction based on FCS-MPC has been proposed and implemented by single-vector control [18], [19], three-vector control [20] and hybrid pulse width modulation (PWM) control [21]. However, due to the randomness of DSVM (single vector, two vectors or three vectors may be applied in one control period), the above methods cannot be directly applied to DSVM based FCS-MPC.

In order to improve the steady-state performance of PMSM driver systems with a low inverter frequency, this paper proposes a double-objective finite control set model-free predictive control using DSVM (DOFCS-MFPC-DSVM). At first, DSVM is used to generate virtual voltage vectors by equally dividing the voltage hexagon. Then model-free deadbeat current control is used to obtain the RVV, and the real-time implementation of the optimal voltage vector (OVV) based on DSVM is overcome. Then a two-level cost function is designed to control the stator currents and to reduce the inverter switching frequency. In this way, double-objective control is realized. The proposed control scheme has been researched through the experiments on a surface-mounted PMSM (SMPMSM) drive system and some valuable conclusions are shown.

II. Ultra-Local Model of a PMSM Drive System

The ultra-local model [4] of a PMSM drive system is established in the synchronous rotating *dq*-coordinates and is given as:

$$\frac{d\boldsymbol{i}_{dq}}{dt} = \boldsymbol{F}_{dq} + \boldsymbol{\alpha}_{dq}\boldsymbol{u}_{dq} \tag{1}$$

where $\boldsymbol{i}_{dq} = \begin{bmatrix} i_d & i_q \end{bmatrix}^T$, $\boldsymbol{F}_{dq} = \begin{bmatrix} F_d & F_q \end{bmatrix}^T$, $\boldsymbol{\alpha}_{dq} = \begin{bmatrix} \alpha_d & 0 \\ 0 & \alpha_q \end{bmatrix}$, $\boldsymbol{u}_{dq} = \begin{bmatrix} u_d & u_q \end{bmatrix}^T$. i_d and i_q are stator currents in the synchronous rotating frame. u_d and u_q represent *dq*-axes voltages. α_d, and α_q are parameters that ensure $d\boldsymbol{i}_{dq}/dt$ and $\boldsymbol{u}_{dq}$ have the same magnitude. $\boldsymbol{F}_{dq}$ contains the known and unknown parts of the PMSM drive system.

F_d and F_q are estimated by the algebraic parameter identification techniques [5] :

$$\begin{cases} \hat{F}_d = -\dfrac{3!}{T_F^3}\int_0^{T_F}\left((T_F - 2\delta)i_d(\delta) + \alpha_d\delta(T_F - \delta)u_d(\delta)\right)d\delta \\ \hat{F}_q = -\dfrac{3!}{T_F^3}\int_0^{T_F}\left((T_F - 2\delta)i_q(\delta) + \alpha_q\delta(T_F - \delta)u_q(\delta)\right)d\delta \end{cases} \tag{2}$$

where $\hat{F}_d(k)$ and $\hat{F}_q(k)$ represent the estimation of F_d and F_q. $T_F = n_F T_s$ is the window sequence length. This means that $\hat{F}_d(k)$ and $\hat{F}_q(k)$ are estimated by the data of $n_F + 1$ periods, and T_s is the sampling period.

Based on the discretization of Equ. (1), the stator currents of the PMSM at the next sampling time can be predicted as:

$$\boldsymbol{i}_{dq}^p(k+1) = \left(\hat{\boldsymbol{F}}_{dq}(k) + \boldsymbol{\alpha}_{dq}\boldsymbol{u}_{dq}(k)\right)T_s + \boldsymbol{i}_{dq}(k) \tag{3}$$

where, $\boldsymbol{i}_{dq}^p(k+1) = \begin{bmatrix} i_d^p(k+1) & i_q^p(k+1) \end{bmatrix}^T$, $\hat{\boldsymbol{F}}_{dq}(k) = \begin{bmatrix} \hat{F}_d(k) & \hat{F}_q(k) \end{bmatrix}^T$, $\boldsymbol{u}_{dq}(k) = \begin{bmatrix} u_d(k) & u_q(k) \end{bmatrix}^T$ and $\boldsymbol{i}_{dq}(k) = \begin{bmatrix} i_d(k) & i_q(k) \end{bmatrix}^T$. In addition, $\hat{F}_d(k)$ and $\hat{F}_q(k)$, including motor parametric uncertainties and inverter nonlinearities, are updated every sampling and can be obtained in [5].

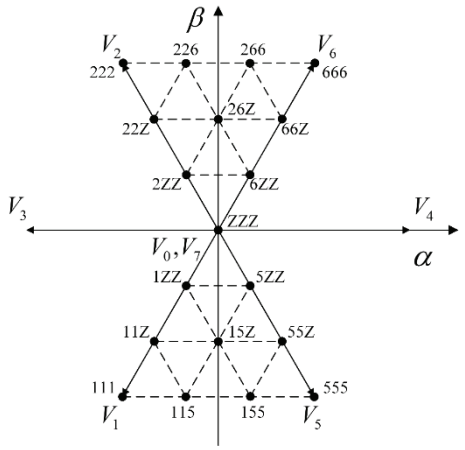

Fig. 1. Discrete space voltage vectors of an inverter.

III. DOFCS-MFPC-DSVM BASED PMSM DRIVE SYSTEM

A. Discrete Space Vector Modulation

It is generally acknowledged that eight basic voltage vectors can be generated by a two-level voltage source inverter, and 100,010,001,110,101,011 are defined as active voltage vectors. In DSVM, the sampling time is equally divided into N parts, and many virtual voltage vectors are generated by applying basic voltage vectors for equal time intervals. Discrete space voltage vectors of an inverter are shown in Fig. 1, where the value of N is 3. The solid dots represent virtual voltage vectors and basic voltage vectors. The label denotes the synthesized voltage vectors. For instance, the label "26Z" represents the virtual voltage vector obtained by applying V_2, V_6 and zero voltage vectors for each equal time interval.

B. Real-time Implementation of OVV based on DSVM

The predictive currents of different voltage vectors can be calculated by Equ. (3), and the results are used to evaluate the cost function to obtain the OVV. However, the iterative process significantly increases the computational burden of the processor. To improve computational efficiency, a real-time implementation of OVV without the evaluation of a cost function is proposed.

The RVV is generated by model-free deadbeat current control and expressed by:

$$\boldsymbol{u}_{dq}^{ref}(k)=\frac{1}{T_s}\boldsymbol{\alpha}_{dq}^{-1}\left(\boldsymbol{i}_{dq}^{*}(k+1)-\boldsymbol{i}_{dq}(k)\right)-\boldsymbol{\alpha}_{dq}^{-1}\hat{\boldsymbol{F}}_{dq}(k) \tag{4}$$

where $\boldsymbol{u}_{dq}^{ref}(k)=\left[u_d^{ref}(k)\quad u_q^{ref}(k)\right]^{\mathrm{T}}$. $u_d^{ref}(k)$, $u_q^{ref}(k)$ are the RVV in synchronous rotating frame.

The RVV is converted into the stationary reference frame using the Park transformation and the result is expressed as $\boldsymbol{u}_{\alpha\beta}^{ref}(k)$. To obtain the OVV, the RVV is synthesized first. A novel calculation method for duty cycles is proposed to extend the voltage constraint to the hexagon without involving trigonometric functions.

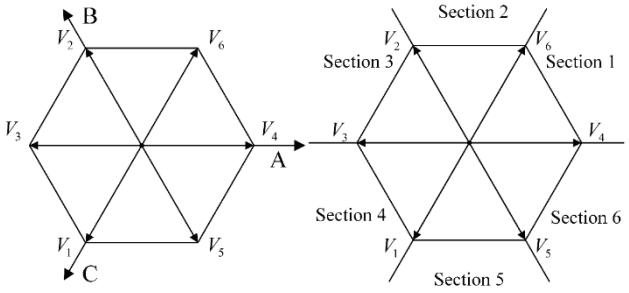

(a) (b)

Fig. 2. Definitions in the $\alpha\beta$ reference frame: (a) A, B and C directions; (b) Six sections.

TABLE I
SIGNS OF THE PRODUCT OF THREE DUTY CYCLE PAIRS AND THE OPTIMAL ACTIVE VECTORS IN SIX SECTIONS

	$d_{a1}^1 d_{a2}^1$	$d_{a1}^2 d_{a2}^2$	$d_{a1}^3 d_{a2}^3$	Optimal Active Vectors
Section 1	>0	<0	>0	V_4, V_6
Section 2	>0	>0	<0	V_6, V_2
Section 3	<0	>0	>0	V_2, V_3
Section 4	>0	<0	>0	V_3, V_1
Section 5	>0	>0	<0	V_1, V_5
Section 6	<0	>0	>0	V_5, V_4

The A, B and C directions in the $\alpha\beta$ stationary reference frame and six sections are shown in Fig. 2, where the phase of the α direction is the same as the A direction. Obviously, $\boldsymbol{u}_{\alpha\beta}^{ref}(k)$ can be synthesized by the voltage vectors in any of the two directions as:

$$\boldsymbol{u}_{\alpha\beta}^{ref}(k)=\begin{cases} d_{a1}^1 V_4 + d_{a2}^1 V_2 \\ d_{a1}^2 V_4 + d_{a2}^2 V_1 \\ d_{a1}^3 V_2 + d_{a2}^3 V_1 \end{cases} \tag{5}$$

where $\boldsymbol{d}^1=\left[d_{a1}^1 \quad d_{a2}^1\right]^T$, $\boldsymbol{d}^2=\left[d_{a1}^2 \quad d_{a2}^2\right]^T$, $\boldsymbol{d}^3=\left[d_{a1}^3 \quad d_{a2}^3\right]^T$. $\boldsymbol{d}^1$, $\boldsymbol{d}^2$, $\boldsymbol{d}^3$ are three duty cycle pairs of active voltage vectors. If the value of the duty cycle is negative, the opposite voltage vector is used.

Then the three pairs of duty cycle are calculated by:

$$\begin{cases} d_{a1}^1=\dfrac{3}{2U_{dc}}\left(u_\alpha^{ref}(k)+\dfrac{u_\beta^{ref}(k)}{\sqrt{3}}\right),\ d_{a2}^1=\dfrac{\sqrt{3}u_\beta^{ref}(k)}{U_{dc}} \\ d_{a1}^2=\dfrac{3}{2U_{dc}}\left(u_\alpha^{ref}(k)-\dfrac{u_\beta^{ref}(k)}{\sqrt{3}}\right),\ d_{a2}^2=-\dfrac{\sqrt{3}u_\beta^{ref}(k)}{U_{dc}} \\ d_{a1}^3=\dfrac{3}{2U_{dc}}\left(-u_\alpha^{ref}(k)+\dfrac{u_\beta^{ref}(k)}{\sqrt{3}}\right),\ d_{a2}^3=-\dfrac{3}{2U_{dc}}\left(u_\alpha^{ref}(k)+\dfrac{u_\beta^{ref}(k)}{\sqrt{3}}\right) \end{cases} \tag{6}$$

where $u_\alpha^{ref}(k)$, $u_\beta^{ref}(k)$ are the values of the RVV in the $\alpha\beta$-axes.

The sign of the product of three duty cycle pairs and the optimal active voltage vectors in six sections are shown in Table I. It is obvious that the optimal active voltage vectors

TABLE II
IDENTIFICATION OF THE SUBSECTION AND TIME INTERVAL NUMBER OF THE ACTIVE VOLTAGE VECTORS OF THE OVV

Subsection of voltage vector space	**The RVV inside of the voltage constraint**			
	I	**II**	**III**	**IV**
conditions	$C_1 \le 0.5, C_2 \le 1$	$C_1 > 0.5, C_3 < 0, C_2 \le 2$	$C_2 > 1, C_3 \ge 0, C_1 \le 1$	$C_1 > 1, C_2 > 2$
$\boldsymbol{n_1}$	n_{a1}^-	n_{a1}^-	n_{a1}^+	n_{a1}^+
$\boldsymbol{n_2}$	n_{a2}^-	n_{a2}^+	n_{a2}^-	n_{a2}^+
Subsection of voltage vector space	**The RVV outside of the voltage constraint**			
	V	**VI**	**VII**	**VIII**	**IX**
conditions	$C_5 \le -N$	C_4 is even.	$C_3 < 0$, C_4 is odd	$C_3 \ge 0$, C_4 is odd	$C_5 \ge N$
$\boldsymbol{n_1}$	0	$(N + C_5)/2$	$(N + C_5 - 1)/2$	$(N + C_5 + 1)/2$	N
$\boldsymbol{n_2}$	N	$(N - C_5)/2$	$(N - C_5 + 1)/2$	$(N - C_5 - 1)/2$	0

$C_1 = 0.5\{n_{a1}\} + \{n_{a2}\}$, $C_2 = 2\{n_{a1}\} + \{n_{a2}\}$, $C_3 = \{n_{a1}\} - \{n_{a2}\}$, $C_4 = n_{a1}^- + n_{a2}^- + N$, $C_5 = n_{a1}^- - n_{a2}^-$.

can be determined by the signs of three duty cycle pairs. When one duty cycle pair has an opposite sign, the corresponding voltage vectors are adjacent the active voltage vectors and selected as the optimal one which defined as $\boldsymbol{d}^{opt} = \begin{bmatrix} d_{a1}^{opt} & d_{a2}^{opt} \end{bmatrix}$.

The number of predefined time intervals of the basic voltage vector is defined as time interval number. For instance, for the virtual voltage vector "446", the time interval number of V_4 is 2 and the time interval number of V_6 is 1. The time interval number of the adjacent active voltage vectors of the RVV are defined as n_{a1} and n_{a2}. n_{a1} and n_{a2} are calculated as:

$$\begin{cases} n_{a1} = \left| d_{a1}^{opt} \right| N \\ n_{a2} = \left| d_{a2}^{opt} \right| N. \end{cases} \tag{7}$$

It is clear that the closest voltage vector of the distance from the RVV minimizes the cost function [18]. The voltage vector space is subdivided based on this principle. Two different conditions with the RVV inside and outside the voltage constraint are analyzed in the following description. In the first case, it is assumed that RVV is located in section 1. According to $n_{a1} \in [k_1, k_1 + 1]$, $n_{a2} \in [k_2, k_2 + 1]$ ($k_1 = 0, 1, \ldots, N\text{-}1$, $k_2 = 0, 1, \ldots, N\text{-}1$), it can be seen that the RVV is located in a parallelogram or triangle surrounded by red lines as shown in Fig. 3(a). and the parallelogram or triangle is subdivided. Obviously, each subsection corresponds to a unique OVV. In the second case, as shown in Fig. 3(b), if the RVV is located on the upper side of l_1 or on the lower side of l_3, the OVV is V_6 or V_4 for the next control period. When the RVV is in the middle area between l_1 and l_2, the OVV is chosen as "466". In order to achieve a unified algorithm, the voltage vector space is subdivided in a way similar to the former case. According to the above analysis, the identification of the subsection and time interval numbers of the active voltage vectors of the OVV can be obtained directly through the RVV as shown in Table II. n_1 and n_2 are

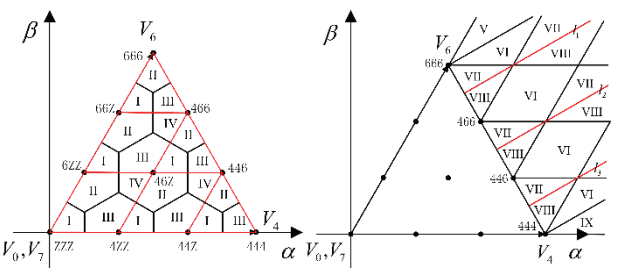

Fig. 3. Subsections of voltage vector space: (a) RVV inside of the voltage constraint; (b) RVV outside of the voltage constraint.

the time interval numbers of the active voltage vectors of the OVV. n_{a1}^+, $n_{\text{-}a1}$ and n_{a2}^+, $n_{\text{-}a2}$ represent the results by rounding up and rounding down n_{a1}, n_{a2}, respectively. $\{x\}$ represent decimal part of x. The identifying conditions in Table II need to be satisfied at the same time. Real-time implementation of the OVV is expressed as:

$$\boldsymbol{u}_{dq}^*(k) = \frac{n_1}{N} V_{a1} + \frac{n_2}{N} V_{a2} \tag{8}$$

where $\boldsymbol{u}_{dq}^*(k)$ denotes the OVV. V_{a1} and V_{a2} represent optimal adjacent active voltage vectors. It should be noted that Equ. (8) and Table II are general expressions for the OVV regardless of the value of N. In transient conditions, the OVV is selected to minimize both of the dq-axes currents tracking errors.

C. Design of a Two-Level Decisional Cost Function

The dq-axes stator currents tracking error is selected as the main control target, and the first-level cost function is defined as:

$$J_i^1 = \left(i_d^*(k+1) - i_d^p(k+1)_i \right)^2 + \left(i_q^*(k+1) - i_q^p(k+1)_i \right)^2 \tag{9}$$

where i = 0,1,2,… represent all of the candidate voltage vectors.

The OVV is calculated by Equ. (8) and the adjacent voltage vectors with their time intervals are obtained through Table I

and Table II. The time interval number of the zero voltage vectors is obtained as $n_0 = n_1 - n_2$. To reduce the inverter switching frequency, the voltage vector sequence is optimized. However, it is complicated to evaluate all of the voltage vector sequences [20] especially for a control system based on DSVM, which applies various basic voltage vectors for a control period. The second-level cost function is designed as shown in Equ. (10), and the new control set is composed of basic voltage vectors, i.e., two adjacent voltage vectors and zero voltage vectors. Since the switching operation of the PWM technique is midpoint symmetric, only the first half of control period needs to be optimized.

$$J_k^2 = \mathrm{S}_k + t_k + z_k \tag{10}$$

where $k = 0,1,2$ represent three basic voltage vectors.

S_k is the commutation number of an inverter from the last switching state to the selected basic voltage vector. In addition, if the last switching state is 000, 100, 010 or 001, the zero voltage vector is chosen to be 000. However, 111 is chosen when the last switching state is 110, 101, 011 or 111.

t_k is the factor to exclude voltage vectors that are not required, i.e., the time interval number is zero. t_k is expressed as:

$$t_k = \begin{cases} 0 & n_k > 0 \\ \infty & n_k = 0. \end{cases} \tag{11}$$

z_k is the factor that ensures that the active voltage vectors are applied prior to the zero voltage vectors when they have the same S_k and t_k. The commutation from an arbitrarily active voltage vector to a zero voltage vector can be chosen from one of the two zero voltage vectors (000, 111). Thus, the commutation number is one. Conversely, it maybe one or two times due to the fixed zero voltage vector. Therefore, the active voltage vectors have a priority for application. For instance, if the required voltage vectors in a control period are zero voltage vectors, 100, 110 and the last switching state is 100, 100 is applied first. However, the commutations are both one when switching state changes from 100 to zero voltage vectors or to 110. Two different conditions have been analyzed. When the second action is the zero voltage vectors, the voltage vector sequence is 100-000-110, and the total switching is three. When the voltage vector sequence is 100-110-111, the commutation of inverter is only two. The expression of z_k is given as:

$$z_k = \begin{cases} 0.5 & k = 0 \\ 0 & k = 1,2. \end{cases} \tag{12}$$

It is obvious that the two adjacent voltage vectors have different J^2, and that the zero voltage vectors are distinguished from the adjacent voltage vectors by z_k. Therefore, although the second cost function is not convex, it still selects the optimal voltage vector. The flowchart of the two-level decisional cost function is shown as Fig. 4. The voltage vector sequence is selected through the iteration of a second-level cost function,

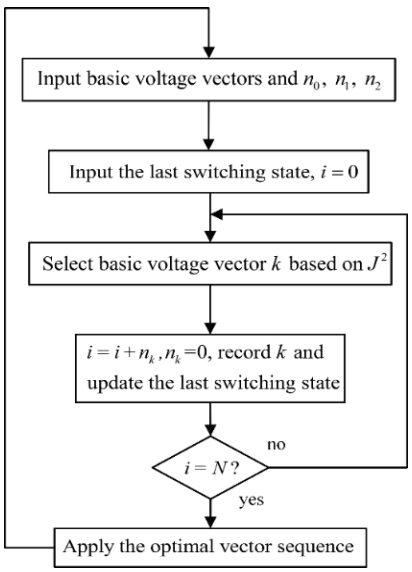

Fig. 4. Flowchart of a two-level decisional cost function.

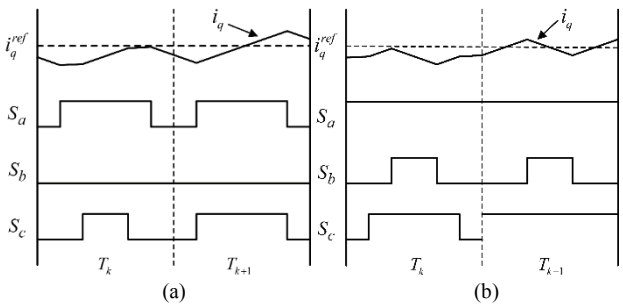

Fig. 5. The inverter switching signal and q-axes stator current waveform: (a) The proposed voltage vector sequence; (b) Five-section PWM.

and the optimal voltage vector sequence is completed until n_0, n_1, n_2 are all set to 0.

D. Switching Frequency Comparison between the Proposed Voltage Vector Sequence and DPWMMIN

DPWMMIN [22] only applies V_0 as the zero voltage vector and this technique is used to minimize the switching frequency in three-vector control [10]. Comparisons of the inverter switching signal and q-axes stator current between the proposed voltage vector sequence and the DPWMMIN is shown in Fig. 5, where the value of N is 3. It is clear that the adjacent voltage vectors are applied at the (k)th control period, and that the commutations of both methods are 4 times. In the next control period, only a single active voltage vector is applied, and the proposed voltage vector sequence reduces the commutation to 3 times. It is clear that the proposed method effectively optimizes the voltage vector sequence. In particular, the q-axes stator current waveforms are similar, which shows that the proposed voltage vector sequence does not affect the current control performance.

Combining the real-time implementation of the OVV and a two-level decisional cost function, the double-objective finite

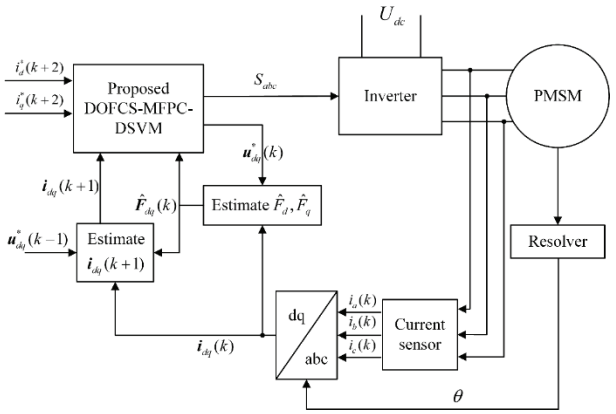

Fig. 6. Control structure diagram of a PMSM drive system based on the proposed DOFCS-MFPC-DSVM.

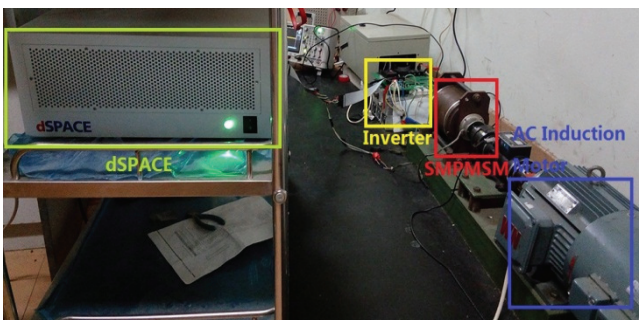

Fig. 7. Experimental bench.

TABLE III
PARAMETERS OF THE TESTED SMPMSM

Parameters	Value
Rated torque	13N·m
Rated current (rms)	19A
Rated speed	500 rpm
Stator resistance	0.0957Ω
dq-axes inductance	1mH
Number of pole-pairs	12
Magnet flux	0.027Wb
Moment of inertia	0.01015kg·m^2

control set predictive current controller is designed. A two-step prediction method is used to compensate the time delay in the actuation. $\hat{F}_{dq}(k) = \hat{F}_{dq}(k+1)$ is assumed due to a sufficiently high sampling frequency. The control structure diagram of a PMSM drive system based on the proposed DOFCS-MFPC-DSVM is shown as Fig. 6.

IV. EXPERIMENTAL RESULTS

In order to verify the effectiveness of the proposed control, experiments have been conducted with a SMPMSM. The experimental bench of a SMPMSM drive system is shown in Fig. 7, and the nominal parameters of the SMPMSM are shown in Table III. dSPACE/DS1007 is used as the controller and it generates the drive signal for the MOSFET-module inverter. The dead-time of the inverter is 2μs. The resolver is used as the rotor position sensor, and the phase current of the SMPMSM is detected by a LEM LA25-P Hall-effect current sensor. The dynamometer is a 2.2-kW AC induction-motor that operates in the speed control mode. The DC-link voltage is 48V. The scaling factors of the *dq*-axes are chosen as $\alpha_d = \alpha_d = 1/L_s = 1000$, and the window length n_F is set to 10.

TABLE IV
TURNAROUND TIMES OF DIFFERENT METHODS

Control method	The iterative method		The method in [16]		The proposed method	
N	3	4	3	4	3	4
Time (μs)	19.8	23.4	12.2	12.2	8.0	8.0

A. Calculation Efficiency Comparison

In order to explore the calculation efficiency of the proposed method, it is compared with both the iterative method [15] and the three candidate voltage vectors method [16]. The turnaround times of the three methods are shown in TABLE IV. Obviously, the proposed method effectively reduces the computing time when compared with the iterative method. Moreover, the turnaround time of the proposed method is 4.2μs smaller than the three candidate voltage vectors method. This test confirms that the proposed method significantly improves calculation efficiency due to the real-time implementation of the OVV, which avoids the enumeration of virtual voltage vectors. Furthermore, increasing *N* does not affect the calculation burden of the proposed method.

B. Performance Comparison between Different Control Methods

The second experiment is the performance comparison between the single-vector control, the three-vector control [10] and the proposed control. For the sake of fairness, the ultra-local model of a PMSM is used in all three methods. The sampling periods of the proposed control and the three-vector control are chosen as 100μs, and the sampling period of the single-vector control is chosen as 50μs. The value of *N* is chosen as 4. To compare the dynamic performances, the *q*-axes stator current step responses of the different control methods are implemented at 100rpm and 400rpm as shown in Fig. 8 and Fig. 9. In the experiments, i_d^* = 0A and i_q^* increases from 0A to 10A at 0.01s. It can be seen that all of three control methods achieve rapid dynamic performance and the difference among them is not significant. Moreover, the *q*-axes stator current rise faster at 100rpm than the current at 400rpm.

In order to compare the steady-state performance, an oscilloscope is used to measure the A-phase stator current as shown in Fig. 10 and Fig. 11. In the experiments, i_d^* = 0A, i_q^*= 10A, and the speed is 100rpm and 400rpm. It is clear that the single-vector control presents a large current harmonic, and

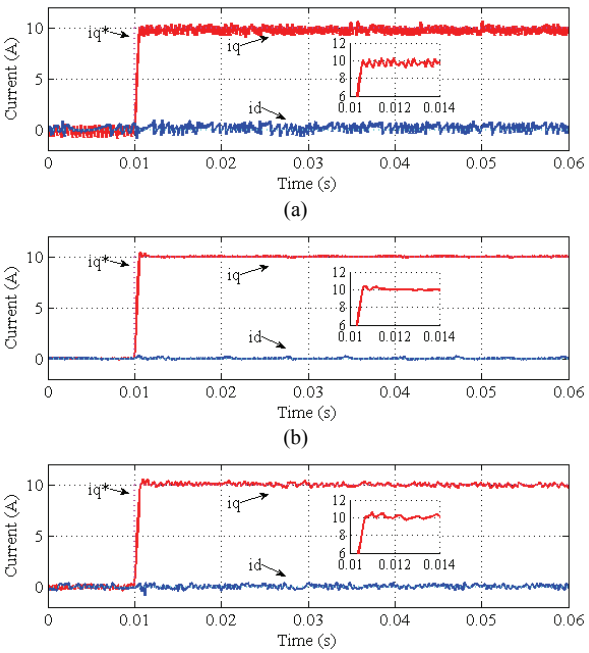

Fig. 8. *dq*-Axes stator current dynamic performance at 100rpm: (a) The single-vector control; (b) The three-vector control; (c) The proposed control, where the value of *N* is 4.

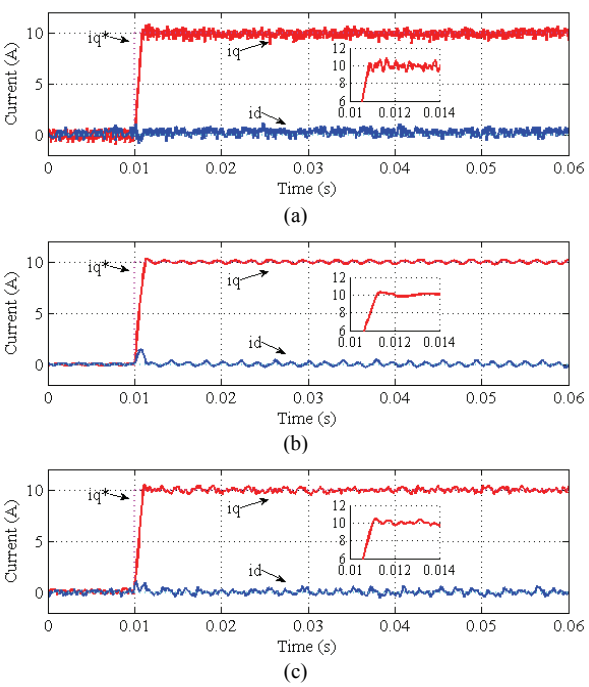

Fig. 9. *dq*-Axes stator current dynamic performance at 400rpm: (a) The single-vector control; (b) The three-vector control; (c) The proposed control, where the value of *N* is 4.

that the three-vector control has a smooth current waveform. Although the proposed control does not show the same current steady-state performance as the three-vector control, it reduces the current ripple effectively when compared with the single-vector control.

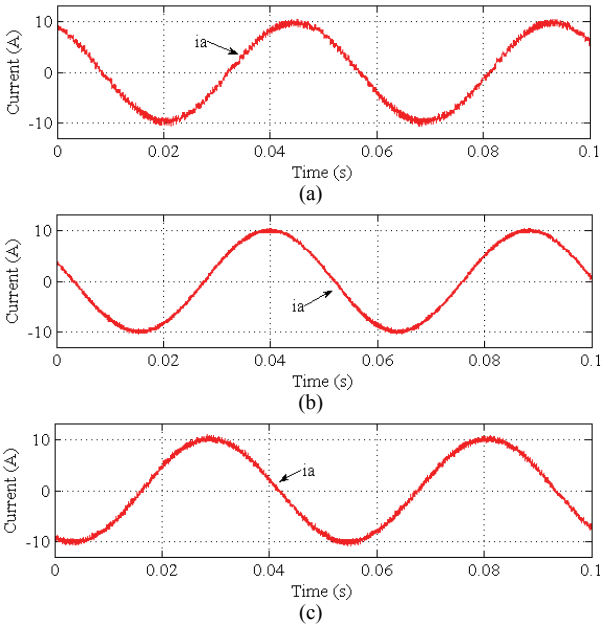

Fig. 10. A-phase stator current steady-state performance at 100rpm; (a) The single-vector control; (b) The three-vector control; (c) The proposed control, where the value of *N* is 4.

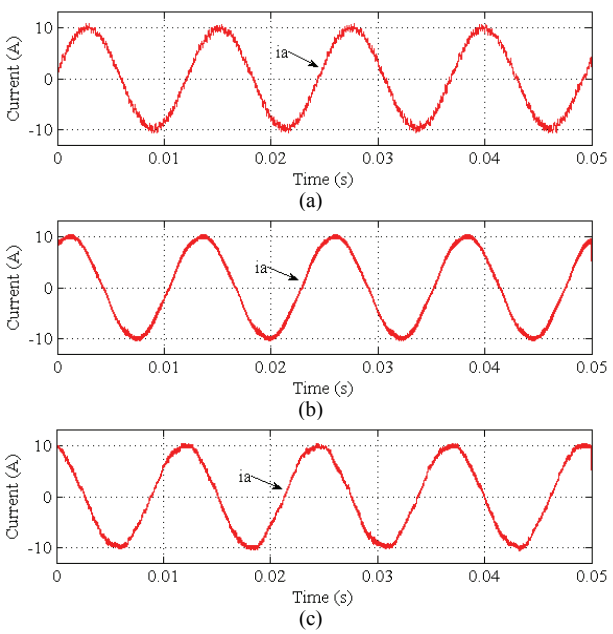

Fig. 11. A-phase stator current steady-state performance at 400rpm: (a) The single-vector control; (b) The three-vector control; (c) The proposed control, where the value of *N* is 4.

To further explore the steady-state performances of the three methods, a comparison of the A-phase current THD and the inverter switching frequency under different rotating speeds are implemented. In the experiments, the *dq*-axes reference currents are i_d^* = 0A and i_q^* =10A. The average switching frequency f_{av} is calculated as [23]:

$$f_{av} = \frac{N_{sum}}{6T} \tag{13}$$

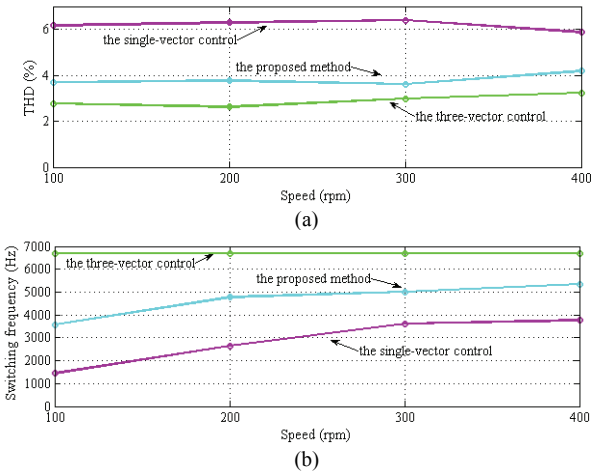

Fig. 12. Steady-state performance comparison between different control methods: (a) THD of the A-phase stator current; (b) Inverter average switching frequency.

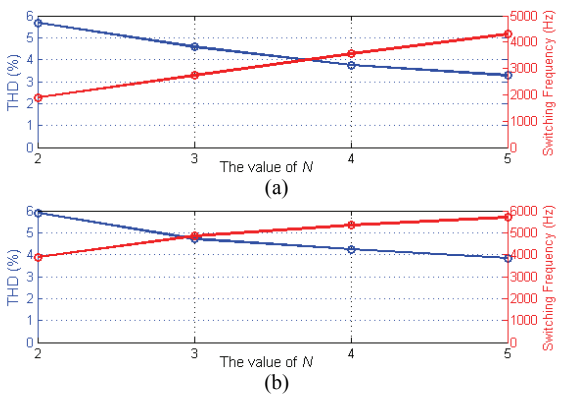

Fig. 13. Steady-state performance of the proposed method with different values of N at: (a) 100rpm; (b) 400rpm.

where N_{sum} is the sum of every power device switching during a predefined period T. T is chosen as 1s for all of the tests.

Experimental results are shown in Fig. 12. Obviously, the three-vector control has the lowest THD. Nevertheless, the switching frequency is 6.67 kHz and it is higher than that of the single-vector control and the proposed method. Although the single-vector control has a low switching frequency, the THD is more than 6% in most cases. The proposed control has fair steady-state performance while restraining the inverter switching frequency, which is considered to be a compromise between the single-vector control and the three-vector control.

C. Influence of N

This experiment analyses the effects of N on the steady-state performance. The THD and the average switching frequency are shown in Fig. 13, where N is increased from 2 to 5. It is clear that with an increase of N, the value of the THD is reduced and the average switching frequency increases gradually. Although more virtual voltage vectors should be considered with the increase of N, the computing time of the proposed method is not increased because of the general expressions for the OVV. This adjustability of N is one of the advantages of the proposed method. As a result, designers can change N online to obtain a desired performance.

TABLE V
COMPARISON OF THE PHASE CURRENT THD (%)

N	3		4	
speed	DPWMMIN	The proposed method	DPWMMIN	The proposed method
100	4.65	4.68	3.68	3.76
200	4.24	4.14	3.81	3.77
300	4.50	4.46	3.60	3.62
400	4.26	4.36	4.20	4.25

TABLE VI
COMPARISON OF THE AVERAGE SWITCHING FREQUENCY (HZ)

N	3		4	
speed	DPWMMIN	The proposed method	DPWMMIN	The proposed method
100	2844	2740	3560	3562
200	4431	4423	5248	4771
300	5687	4957	5949	5010
400	5700	4843	5856	5349

D. Switching Frequency Comparison between the Proposed Voltage Vector Sequence and DPWMMIN

To verify the effectiveness of the switching frequency reduction for the proposed voltage vector sequence, a comparison with DPWMMIN is implemented. It should be noted that the only difference is the voltage vector sequence applied in the control period. The phase current THD value and the average switching frequency of the two methods are shown in Table V and Table VI, respectively. It can be seen that the two methods have almost the same THD of the A-phase stator current under different operation conditions. However, the switching frequency of the proposed voltage vector sequence is reduced in most cases, and the results are identical to the theoretical analysis. At 100rpm, the proposed method has a similar switching frequency to DPWMMIN. It is reasonable that the amplitude of the RVV is small at low speeds, which results in a situation where the zero voltage vectors are always applied in the control period. Therefore, the adjacent control periods are connected by zero voltage vectors, and the proposed method has features similar to those of DPWMMIN.

E. Comparison between Different Methods under Parametric Uncertainties

The last test evaluates the robustness of the proposed method. The proposed method is compared with the model-based method, which predicts the stator currents through a mathematical model of SMPSM, and the rest of the two

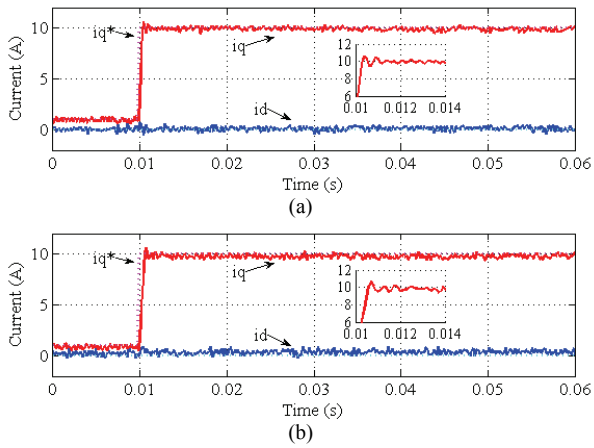

Fig. 14. *dq*-Axes stator currents dynamic performance of the model-based method: (a) At 100rpm; (b) At 400rpm.

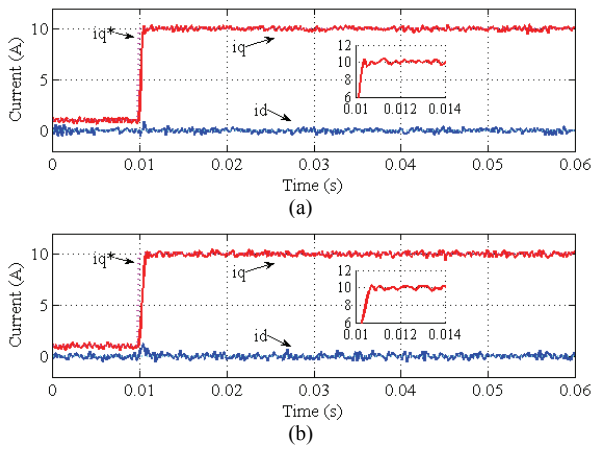

Fig. 15. *dq*-Axes stator current dynamic performance of the proposed method: (a) At 100rpm; (b) At 400rpm.

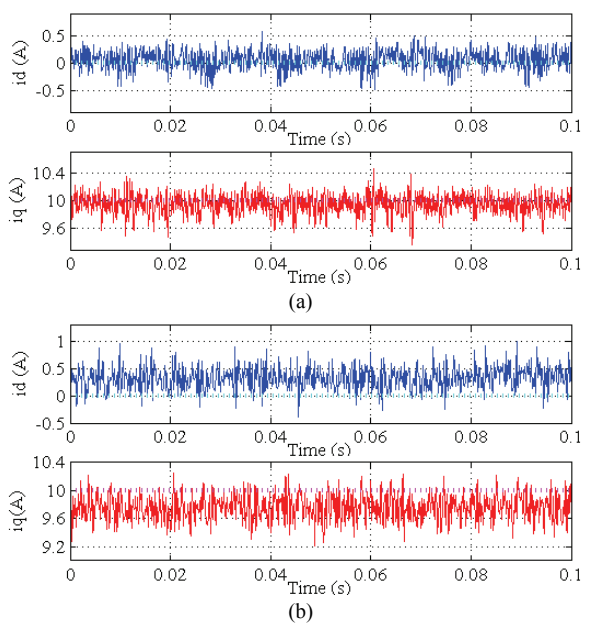

Fig. 16. Steady-state performance of the model-based method: (a) i_{dq} at 100rpm; (b) i_{dq} at 400rpm.

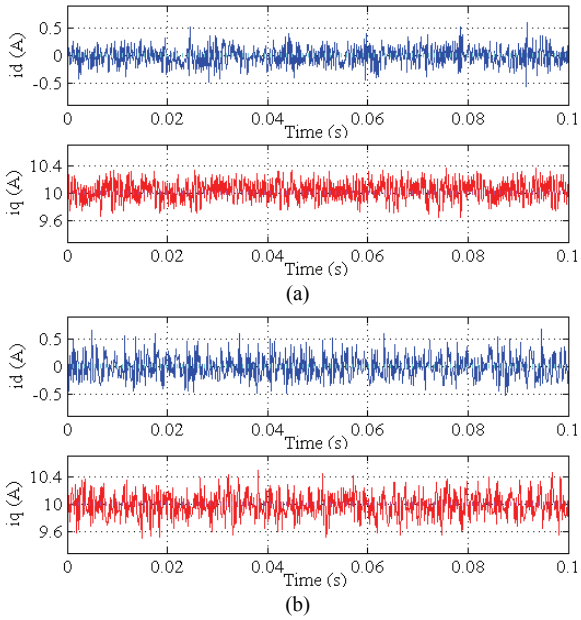

Fig. 17. Steady-state performance of the proposed method: (a) i_{dq} at 100rpm; (b) i_{dq} at 400rpm.

methods are the same.

Comparisons of step current responses are shown in Fig. 14 and Fig. 15. The motor parameters for the model-based method are set as $R = 1.4R_s$, $L = 1.2L_s$ and $\psi = 0.8\psi_f$. The control parameter of the proposed method is chosen as $\alpha_d = \alpha_d = 1/1.2L_s = 833$. In experiments, $i_d^* = 0$A, i_q^* increases from 1A to 10A at 0.01s, and the speeds are 100rpm and 400rpm. As can be seen, both of the methods have fast dynamic response. Moreover, the proposed method has a smaller overshoot. Fig. 16 and Fig. 17 show the steady-state performances of the *dq*-axes stator currents. It can be seen that the influence of parametric uncertainties is insignificant at 100rpm. However, the model-based method has a current tracking error at 400rpm and the proposed method can effectively track the current reference. It is proved that the parametric uncertainties can be compensated by $\hat{F}_d$, $\hat{F}_q$ and the proposed method has strong robustness to variations of system parameters.

V. Conclusions

This paper proposes a double-objective finite control set model-free predictive control using DSVM for PMSM drive systems. DSVM is used to reduce the stator current ripple of a PMSM drive system, and the RVV is obtained by using model-free deadbeat current control. Based on the principle of minimum distance, the voltage vector space is subdivided into nine subsections. The OVV can be obtained directly from a subsection of the RVV. The real-time implementation of the OVV is solved effectively, which avoids the complicated iterative process of the cost function. Therefore, the computational efficiency is significantly improved. Moreover,

to further reduce the inverter switching frequency, a two-level decisional cost function is designed to automatically optimize the voltage vector sequence. Experimental results show that the proposed method reduces the calculation time by 60% when compared with the conventional iteration method. The switching frequency of an inverter controlled by the proposed voltage vector sequence is reduced by approximately 10% compared with DPWMMIN when the PMSM drive system operates at medium and high speeds. With the increase of N, the phase current THD is reduced and the average switching frequency increases. The proposed method shows a rapid dynamic response, small steady-state current ripple and strong robustness due to the accurate ultra-local model of the PMSM drive system. Multi-step prediction and asymmetric zero voltage vectors application, which are useful in the process of optimizing the voltage vector sequence, may be explored in a future paper.

ACKNOWLEDGMENT

This work was supported by the National Natural Science Foundation of China (Grant number: 51877064 and 51377041).

REFERENCES

[1] M. Rivera, J. Rodriguez, and S. Vazquez, "Predictive control in power converters and electrical drives – Part 1," *IEEE Trans. Ind. Electron.*, Vol. 63, No. 6, pp. 3834-3836, Jun. 2016.

[2] S**.** Vazquez**,** J. Rodriguez, M. Rivera, L. G. Franquelo, and M. Norambuena, "Model predictive control for power converters and drives: Advances and trends," *IEEE Trans. Ind. Electron.*, Vol. 64, No. 2, pp. 935-947, Feb. 2017.

[3] S. Bolognani, S. Bolognani, L. Peretti, and M. Zigliotto, "Design and implementation of model predictive control for electrical motor drives," *IEEE Trans. Ind. Electron.*, Vol. 56, No. 6, pp. 1925-1936, Jun. 2009.

[4] M. Fliess and C. Join, "Model-free control," *Int. J. Contr.*, Vol. 86, No. 12, pp. 2228-2252, Jul. 2013.

[5] Y. Zhou, H. Li, and H. Zhang, "Model-free deadbeat predictive current control of surface mounted permanent magnet synchronous motor drive system," *J. Power Electron.*, Vol. 18, No. 1, pp. 103-115, Jan. 2018.

[6] X. Lin-Shi, F. Morel, A. M. Llor, B. Allard, and J. Retif, "Implementation of hybrid control for motor drives" *IEEE Trans. Ind. Electron.*, Vol. 54, No. 4, pp. 1946-1952, Aug. 2007.

[7] Y. Zhang, W. Xie, Z. Li, and Y. Zhang, "Model predictive direct power control of a PWM rectifier with duty cycle optimization," *IEEE Trans. Power Electron.*, Vol. 28, No. 11, pp. 5343-5351, May 2013.

[8] S. Wang, C. Xia, X. Gu, and W. Chen, "A novel FCS-model predictive control algorithm with duty cycle optimization for surface-mounted PMSM," in *Proceeding 7th IET International Conference on Power Electronics*, Machines and Drives, pp. 1-6, 2014.

[9] K. Shyu, J. Lin, V. Pham, M. Yang, and T. Wang, "Global minimum torque ripple design for direct torque control of induction motor drives," *IEEE Trans. Ind. Electron.*, Vol. 57, No. 9, pp. 3148-3156, Sep. 2010.

[10] X. Wang and D. Sun, "Three-vector-based low-complexity model predictive direct power control strategy for doubly fed induction generators" *IEEE Trans. Power Electron.*, Vol. 32, No. 1, pp. 773-782, Jan. 2017.

[11] S. Vazquez, A. Marquez, R. Aguilera, D. Quevedo, J. I. Leon, and L. G. Franquelo, "Predictive optimal switching sequence direct power control for grid-connected power converters," *IEEE Trans. Ind. Electron.*, Vol. 62, No. 4, pp. 2010-2020, Apr. 2015.

[12] E. Fuentes, C. A. Silva, and R. M. Kennel, "MPC implementation of a quasi-time-optimal speed control for a PMSM drive, with inner modulated-FS-MPC torque control," *IEEE Trans. Ind. Electron.*, Vol. 63, No. 6, pp. 3897-3905, Jun. 2016.

[13] Q. Liu and K. Hameyer, "Torque ripple minimization for direct torque control of PMSM with modified FCSMPC," *IEEE Trans. Ind. Appl.*, Vol. 52, No. 6, pp. 4855-4864, Nov./Dec. 2016.

[14] D. Casadei, G. Serra, and K. Tani, "Implementation of a direct torque control algorithm for induction motors based on discrete space vector modulation," *IEEE Trans. Power Electron.*, Vol. 15, No. 4, pp. 769-777, Jul. 2000.

[15] S. Vazquez, J. I. Leon, L. G. Franquelo, J. M. Carrasco, O. Martinez, J. Rodriguez, P. Cortes, and S. Kouro, "Model predictive control with constant switching frequency using a discrete space vector modulation with virtual state vectors," in *Proceeding IEEE International Conference on Industrial Technology*, pp. 1-6, 2009.

[16] Y. Wang, X. Wang, W. Xie, F. Wang, M. Dou, R. M. Kennel, R. D. Lorenz, and D. Gerling, "Deadbeat model predictive torque control with discrete space vector modulation for PMSM drives," *IEEE Trans. Ind. Electron.*, Vol. 64, No. 5, pp. 3537-3547, May 2017.

[17] F. L. Mapelli, D. Tarsitano, and M. Mauri, "Plug-in hybrid electric vehicle: Modeling, prototype realization, and inverter losses reduction analysis," *IEEE Trans. Ind. Electron.*, Vol. 57, No. 2, pp. 598-607, Feb. 2010.

[18] J. Hu, J. Zhu, G. Lei, G. Platt, and D. G. Dorrell, "Multi-objective model-predictive control for high-power converters" *IEEE Trans. Energy Convers.*, Vol. 28, No. 3, pp. 652-663, Sep. 2013.

[19] M. Preindl, E. Schaltz, and P. Thogersen, "Switching frequency reduction using model predictive direct current control for high-power voltage source inverters," *IEEE Trans. Ind. Electron.*, Vol. 58, No. 7, pp. 2826-2835, Jul. 2011.

[20] Y. Zhang and J. Zhu, "A novel duty cycle control strategy to reduce both torque and flux ripples for DTC of permanent magnet synchronous motor drives with switching frequency reduction," *IEEE Trans. Power Electron.*, Vol. 26, No. 10, pp. 3055-3067, Oct. 2011.

[21] M. Gendrin, J. Gauthier, and X. Lin-Shi, "A finite control set model predictive control based hybrid PWM technique," in *proceeding of IEEE International Conference on Industrial Technology*, pp. 2218-2223, 2015.

[22] A. M. Hava, R. J. Kerkman, and T. A. Lipo, "Simple analytical and graphical methods for carrier-based PWM-

VSI drives," *IEEE Trans. Power Electron.*, Vol. 14, No. 1, pp. 49-61, Jan. 1999.

[23] Y. Yan, S. Wang, C. Xia, H. Wang, and T. Shi, "Hybrid control set-model predictive control for field-oriented control of VSI-PMSM," *IEEE Trans. Energy Convers.*, Vol. 31, No. 4, pp. 1622-1633, Dec. 2016.

Beishi Zhao was born in Anhui, China, in 1994. He received his B.S. degree in Electrical Engineering from Nanjing Tech University, Nanjing, China, in 2016. He is presently working towards his M.S. degree in the Department of Electrical Engineering and Automation, Hefei University of Technology, Hefei, China. His current research interests include power electronics and predictive control of electrical motor drives.

Hongmei Li was born in Anhui, China, in 1969. She received her B.S. and M.S. degrees in Electrical Engineering from Hefei University of Technology, Hefei, China, in 1991 and 1996, respectively. She received her Ph.D. degree in Electrical Engineering from the Shenyang University of Technology, Shenyang, China, in 2003. She has been a Professor in the Department of Electrical Engineering, Hefei University of Technology, since 2006. Her current research interests include power electronics and motor control, fault diagnosis, and fault-tolerant control of electrical machine systems.

Jingkui Mao was born in Henan, China, in 1978. He received his B.S. degree in Automation from Central South University of Technology, Changsha, China, in 2002. He is presently working towards his Ph.D. degree in the Department of Electrical Engineering and Automation, Hefei University of Technology, Hefei, China. He is presently working as an Associate Professor of Henan Institute of Technology. His current research interests include predictive control and discrete space vector modulation of electrical motor drives.